Applied Catalysis B: Environmental 89 (2009) 543–550

Contents lists available at ScienceDirect

Applied Catalysis B: Environmental

journal homepage: www.elsevier.com/locate/apcatb

Highly active $TiO_{2-x-y}N_xF_y$ visible photocatalyst prepared under supercritical conditions in NH_4F/EtOH fluid

Yuning huo, Yi jin, Jian zhu, Hexing li *

Department of Chemistry, Shanghai Normal University, Shanghai 200234, China

ARTICLE INFO

Article history:
Received 12 September 2008
Received in revised form 2 January 2009
Accepted 22 January 2009
Available online 2 February 2009

Keywords:
$TiO_{2-x-y}N_xF_y$ visible photocatalyst
Supercritical treatment
NH_4F/ethanol fluid
Photodegradation of methylene blue
Synergetic promoting effects

ABSTRACT

A novel N and F co-doped TiO_2 ($TiO_{2-x-y}N_xF_y$) photocatalyst is prepared by treating the TiO_2 precursor in NH_4F/ethanol fluid under supercritical conditions. During photocatalytic degradation of methylene blue under visible light irradiation, the as-prepared $TiO_{2-x-y}N_xF_y$ exhibits higher activity than the undoped TiO_2, N-doped TiO_2 ($TiO_{2-x}N_x$), and F-doped TiO_2 ($TiO_{2-y}F_y$). Based on the characterizations including XRD, Raman, FTIR, TEM, PLS, UV–vis DRS, N_2 adsorption–desorption isotherms, XPS and NH_3-TPD, the synergetic promotions of N- and F-dopants incorporated into the TiO_2 lattice are discussed based on the enhanced spectral response in visible region, oxygen vacancies, and surface acidic sites. Meanwhile, the supercritical treatment also promotes the activity owing to the increase in both the surface area and the crystallization degree of anatase, and the enhanced incorporation of N- and F-dopants into the TiO_2 lattice.

1. Introduction

Photocatalysis has caused much attention owing to its potential in dealing with environmental pollution and generating clean hydrogen energy. However, the pure TiO_2 with energy band gap of 3.2 eV exhibits spectral response only in UV region, which limits the practical applications due to the poor utilization of solar lights [1–4]. Doping TiO_2 with nitrogen [5–8], sulphur [9–11], fluorine [12–13], and carbon impurities [14–16] has been frequently employed for achieving visible photocatalysts. Among various doped TiO_2 samples, the N-doped TiO_2 ($TiO_{2-x}N_x$) has been most thoroughly studied owing to its strong spectral response in visible region [17–19]. The F-doped TiO_2 ($TiO_{2-y}F_y$) also displays high activity owing to the enhanced surface acidic sites [20], which are favorable for adsorbing reactant molecules and also inhibiting the recombination between photoelectrons and holes, leading to the enhanced quantum efficiency. Up to now, all the N- and/or F-doped TiO_2 samples have been synthesized based on sol–gel route [13,21–22], chemical vapor deposition [23], spray pyrolysis [24–25], and ion implantation [17–26]. To ensure the incorporation of F and N-dopants into the TiO_2 lattice, all these processes should be conducted at high temperature, leading to the limited content of dopants and also the low surface area due to particle agglomeration and pore collapse [27–28]. Preparation of doped TiO_2 photocatalysts under supercritical conditions could preserve the porous materials and high surface area in the precursor owing to the lack of surface tension [29]. Meanwhile, the high pressure and temperature under supercritical conditions may also enhance crystallization degree of anatase and promote the incorporation of dopants into the TiO_2 lattice [29–31], leading to the high quantum efficiency. Previously, we reported N-, S- and B-doped TiO_2 visible photocatalysts prepared via supercritical treatment, which showed higher activities than the corresponding ones obtained by direct calcinations [32–35]. However, the activity is still limited by the low content of the dopants and thus, co-doped TiO_2 should be considered. Herein, we reported a new N and F co-doped TiO_2 photocatalyst ($TiO_{2-x-y}N_xF_y$) prepared by treating the TiO_2 precursor in NH_4F/ethanol fluid under supercritical conditions. Owing to the synergetic promoting effects from the N- and F-dopants, such catalyst exhibited very high activity during photocatalytic degradation of MB under visible light irradiation. The catalyst could be recycled easily and used repetitively, showing a good potential in practical applications.

2. Experimental

2.1. Catalyst preparation

A solution comprised of 2.5 mL 1.0 M HNO_3 solution and 10.0 mL ethanol is added dropwise within 20 min into another solution consisting of 10.0 mL $Ti(O\text{-}C_4H_9)_4$ and 40.0 mL ethanol at 313 K under vigorous stirring. The solution is stirred continuously

* Corresponding author. Fax: +86 21 64322272.
E-mail address: HeXing-Li@shnu.edu.cn (H. li).

0926-3373/$ – see front matter © 2009 Elsevier B.V. All rights reserved.
doi:10.1016/j.apcatb.2009.01.019

for 60 min until the formation of TiO_2 gel. After being aged for 48 h at 313 K, the TiO_2 xerogel is transferred into a 500 mL autoclave containing 250 mL ethanol and desired amount of NH_4F, where the system is treated under the supercritical conditions (553 K, 13.5 MPa) for 2 h. Then, the vapor is released slowly and the system is allowed to cool down to room temperature in the N_2 flow. The obtained solid is calcined for 4 h to remove the residual organic compounds and the solvent. In most cases, the calcination temperature is fixed at 773 K. Finally, the as-prepared samples are crushed and kept in vacuum until the time of use. The TiO_2 samples doped with different N- and F-contents could be obtained by adjusting the NH_4F concentration in the supercritical fluid and denoted as $TiO_{2-x-y}N_xF_y$(SC)–X, where SC refers to supercritical treatment, and X = 1, 2, 3, 4, 5 corresponding to the NH_4F concentration of 0.06, 0.12, 0.24, 0.48, and 0.96 M, respectively. For comparison, the $TiO_{2-x}N_x$(SC) and $TiO_{2-y}F_y$(SC) are also synthesized in the similar way by using either triethylamine (Et_3N)/ethanol or HF/ethanol as the supercritical fluid. Meanwhile, the $TiO_{2-x-y}N_xF_y$(DC) is prepared by impregnating the TiO_2 precursor in NH_4F solution overnight, followed by direct calcination at 773 K for 4 h. The P25 TiO_2 is commercially available and used without further treatment.

2.2. Catalyst characterization

The catalyst structure is investigated by X-ray diffraction (XRD, Rigacu Dmax-3C, Cu Kα radiation), selected area electronic diffractions (SAED, JEM-2010), Raman spectrometer (Dilor Super LabRam II), and Fourier transform infrared (FTIR, NEXUS 470). The grain size is calculated by using Scherrer's equation based on the principal XRD peak. Surface morphology and particle size are observed through transmission electronic micrography (TEM, JEM-2010). The light absorbance is measured by photoluminescence spectra (PLS, Varian Cary-Eclipse 500) and UV–vis diffuse reflectance spectra (DRS, MC-2530). N_2 adsorption–desorption isotherms are measured on a NOVA 4000 at 77 K, from which the surface area (S_{BET}), pore volume (V_P), and average pore diameter (d_P) are calculated by using BJH method. The surface electronic states are analyzed by X-ray photoelectron spectroscopy (XPS, Versa Probe PHI 5000). All the binding energy (BE) values are calibrated by using the standard BE value of contaminant carbon (C_{1s} = 284.6 eV) as a reference. The molar ratios of N/Ti and/or F/Ti in various doped TiO_2 samples are determined based on the areas of the XPS peaks characteristic of N, F, and Ti by using 0.477, 1.000 and 2.001 as the PHI sensitivity factors [36]. Temperature-programmed desorption of ammonia (NH_3-TPD) is carried out in a self-designed system according to following procedures. 0.10 g sample is pretreated under a helium flow (30 mL/min) at 773 K for 1 h. After cooling to 333 K, the system is saturated with pure NH_3 gas, following by keeping at 393 K for 1 h to remove physisorbed gases. Then, the temperature is raised from 393 K to 793 K at ramp rate of 10 K/min and the NH_3 desorbed is quantitatively determined by a gas chromatograph (GC122).

2.3. Activity test

The photocatalytic degradation of methylene blue (MB) is carried out at 303 K in a self-designed 100 mL glassy reactor containing 0.050 g catalyst and 50.0 mL of 0.010 g/L MB aqueous solution. The reaction system is stirred vigorously (> 800 rpm) to eliminate diffusion effect on the reaction kinetics. Keeping the mixture for more than 1 h to reach adsorption equilibrium (Fig. S1), the photocatalytic reaction is initiated by irradiating with a 500 W Xenon lamp (CHF-XM500, light intensity = 600 mW/cm^2) located at 18 cm above the solution. To make sure that the photocatalytic reaction is really driven by visible lights, all the UV lights with wavelength lower than 420 nm are removed by a glass filter (JB-420). Each run of the reactions is lasted for 3 h and the MB left in the solution is analyzed by a UV spectrophotometer (UV 7504/PC) at its characteristic wavelength (λ = 665 nm) [18]. Besides CO_2, no other organic products have been identified by HPLC–MS, indicating the complete MB decomposition under the present reaction conditions. Preliminary tests show that there is a good linear relationship between the light absorbance and the concentration of organic compounds. Meanwhile, experimental results also confirm that only less than 9.0% MB decomposed after reaction for 3 h in the same conditions in the absence of either the photocatalyst or the light irradiation (see Fig. S1 and Fig. S2), and thus, could be neglected in comparison with the photocatalysis process. The reproducibility of the results is checked by repeating the experiments at least three times and is found to be within acceptable limits (±5%).

The catalyst durability is measured according to the following procedure. After each run of photocatalysis reactions, the photocatalyst is separated from aqueous solution by centrifugation, washed with H_2O for three times and dried at 373 K for 12 h. Then, each recycling test is conducted under the same conditions for 3 h and the MB degradation yield is determined to show the change of activity.

3. Results and discussion

As shown in Fig. 1, the FTIR spectra reveal that all the undoped and doped TiO_2 samples display absorbance bands around 3410, 1630, and 580 cm^{-1} indicative of the O–H bending vibration [37–38] and the stretching vibration of the O–Ti bonds [39]. In comparison with the undoped TiO_2(SC), the $TiO_{2-x-y}N_xF_y$(SC)-3 displays additional four absorbance peaks. The peaks around 1450, 1220 and 1160 cm^{-1} are attributed to the vibrations of the N–Ti bond, while the peak at 1390 cm^{-1} is resulted from the vibration of surface-adsorbed NH_3 [33,40–42]. These characteristic peaks are also observed in the $TiO_{2-x}N_x$(SC) sample. Besides, the $TiO_{2-x-y}N_xF_y$(SC)-3 also shows peak around 460 cm^{-1} indicative of the vibration of the F–Ti bond [43,44], which could also be found in the $TiO_{2-y}F_y$(SC). This peak is partially overlapped by the absorbance peak of the O–Ti bonds. The appearance of the N–Ti and F–Ti bonds suggests the incorporation of N- and/or F-dopants into the TiO_2 lattice under supercritical conditions.

The XPS spectra are employed to show whether the N–Ti–N and the F–Ti–F bonds or the O–Ti–N and the O–Ti–F bonds are formed

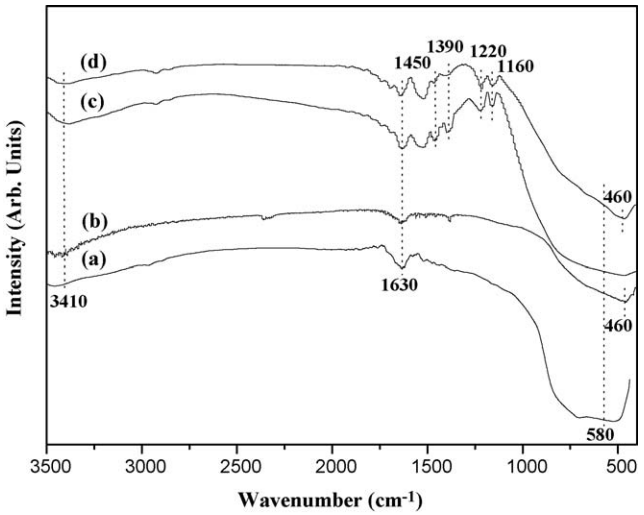

Fig. 1. FTIR spectra of (a) TiO_2(SC), (b) $TiO_{2-y}F_y$(SC), (c) $TiO_{2-x}N_x$(SC) and (d) $TiO_{2-x-y}N_xF_y$(SC)-3 samples calcined at 773 K.

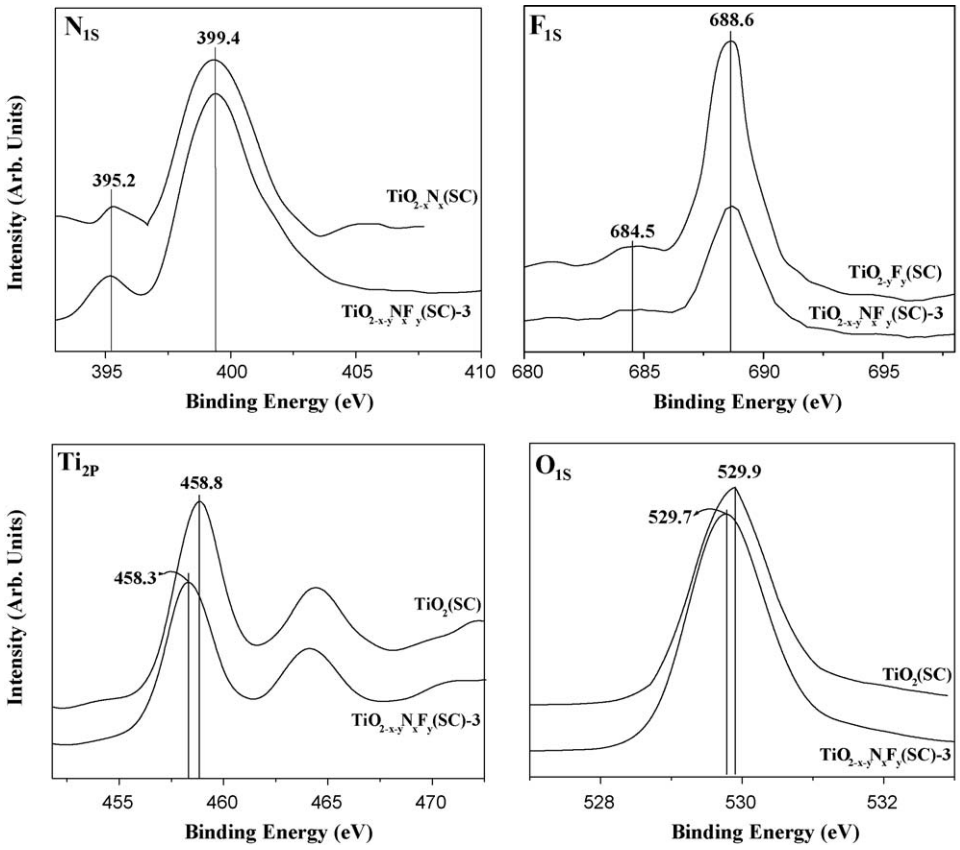

Fig. 2. XPS spectra of different samples calcined at 773 K.

in the F- and/or N-doped TiO_2 samples. As shown in Fig. 2, both the $TiO_{2-x-y}N_xF_y$(SC)-3 and the $TiO_{2-x}N_x$(SC) samples display two kinds of N species. Up to now, the assignment of the XPS peak of N_{1S} has still been under debate. Some papers [45,46] claimed that the peak around 396 eV should be the N in the TiO_2 lattice while the peak around 400 eV should be to the chemisorbed N species. However, Chen and Burda [47] argued that the N incorporated into the lattice should locate around 400 eV. Recently, Zhang and co-workers [48] measured the XPS spectra of N-doped and N/Fe-co-doped TiO_2, and suggested that the N_{1S} peak around 399 eV can be attributed to the substitutional nitrogen replaced one O atom of the lattice, which was consistent with previous conclusion [49,50]. The preparation methods and conditions largely affect nitrogen XPS spectral features and thus the peak position may be different in the literatures. The former conclusion has been drawn based the N-doped obtained via calcination at high temperature in N_2 flow. While, the latter conclusion is drawn based the N-doped obtained via treating the TiO_2 precursor in ammonium solution under hydrothermal conditions or other similar methods. Since the $TiO_{2-x-y}N_xF_y$(SC) and $TiO_{2-x}N_x$(SC) samples are prepared based on supercritical treatment which is similar to the hydrothermal treatment, the peak around 400 eV can be assigned to the N species in the O–Ti–N bond while the peak around 396 eV is assigned to the adsorbed N species (e.g., NH_3), which is further confirmed by the XPS spectrum of the TiO_2 sample after being impregnated with NH_3 solution but without supercritical treatment (Fig. S3). Accordingly, Fig. 2 demonstrates that, besides trace of surface-adsorbed NH_3 molecules with the binding energy (BE) around 395.2 eV, most N species are present in O–Ti–N bonds rather than N–Ti–N bonds, corresponding to the BE around 399.4 eV [47]. Calcination of the $TiO_{2-x-y}N_xF_y$(SC)-3 at elevated temperature causes a gradual decrease in intensity of the peak around 395.2 eV due to desorption of the surface-adsorbed N species, but the peak around 399.4 eV remains unchanged since the N species in the O–Ti–N bond are difficult to be removed (see Fig. S4). The surface-adsorbed F species and O–Ti–F bonds are also identified in both the $TiO_{2-x-y}N_xF_y$(SC)-3 and the $TiO_{2-y}F_y$(SC), corresponding to the BE around 684.5 and 688.6 eV [51,52], respectively. In comparison with the undoped TiO_2(SC), the $TiO_{2-x-y}N_xF_y$(SC)-3 displays negative BE shift in either the $Ti_{2P3/2}$ or the O_{1S} level, which further confirms the formation of O–Ti–N and O–Ti–F bonds. Based on the areas of principal XPS peaks indicative of Ti, N and F, the real

Table 1
Structure parameters and photocatalytic activities of different catalysts[a].

Catalyst	Molar ratio (%)		S_{BET} (m^2/g)	V_P (cm^3/g)	Degradation yield (%)
	N/Ti	F/Ti			
P25 TiO_2	0	0	45	0.20	10
TiO_2(DC)	0	0	23	0.03	7
TiO_2(SC)	0	0	78	0.21	11
$TiO_{2-y}F_y$(SC)	0	1.5	86	0.21	64
$TiO_{2-y}F_y$(SC)-1	0	4.0	86	0.23	62
$TiO_{2-x}N_x$(SC)	2.4	0	102	0.26	76
$TiO_{2-x}N_x$(SC)-1	4.0	0	107	0.29	78
$TiO_{2-x-y}N_xF_y$(SC)-1	1.2	0.7	88	0.29	60
$TiO_{2-x-y}N_xF_y$(SC)-2	2.0	1.2	94	0.34	80
$TiO_{2-x-y}N_xF_y$(SC)-3	2.4	1.7	103	0.37	87
$TiO_{2-x-y}N_xF_y$(SC)-4	2.7	2.1	109	0.41	84
$TiO_{2-x-y}N_xF_y$(SC)-5	3.1	2.4	114	0.48	82
$TiO_{2-x-y}N_xF_y$(DC)	1.0	0.6	52	0.03	42
Mixture[b]	2.4	1.6	97	0.31	60

[a] Reaction conditions: 0.050 g catalyst, 50.0 mL 0.010 g/L MB, a 500 W Xenon lamp (light intensity = 600 mW/cm^2, wavelength > 420 nm), reaction temperature = 303 K, stirring rate > 800 rpm, reaction time = 3 h.

[b] Obtained by mixing $TiO_{2-x}N_x$(SC)-1 and $TiO_{2-y}F_y$(SC)-1 in the molar ratio of 3/2, which ensures the same N- and F-contents as those in the $TiO_{2-x-y}N_xF_y$(SC)-3.

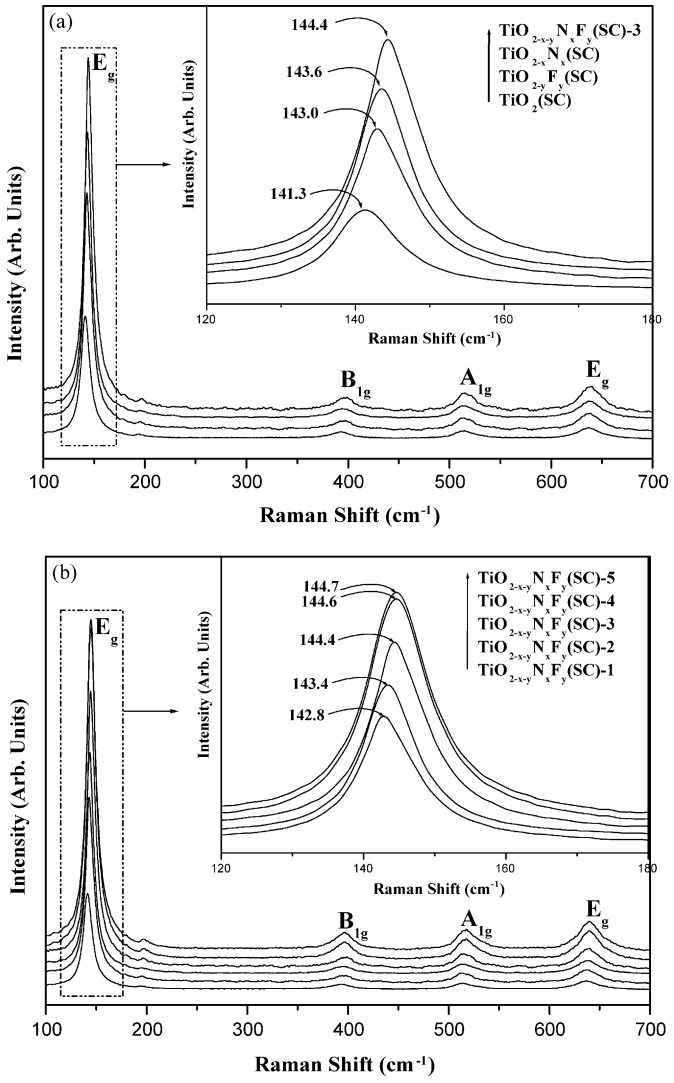

Fig. 3. Raman spectra of different samples calcined at 773 K.

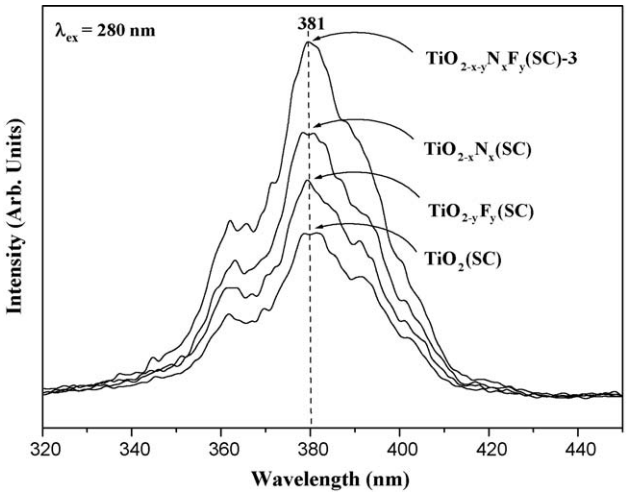

Fig. 4. PL spectra of different samples calcined at 773 K.

N/Ti and/or F/Ti molar ratios in the doped TiO_2 are calculated and listed in Table 1.

The incorporation of the N- and F-dopants into the TiO_2 lattice could be further confirmed by Raman spectra. As shown in Fig. 3(a), all the doped and undoped TiO_2 samples calcined at 773 K are present in pure anatase phase, corresponding to Raman modes of E_g, B_{1g}, A_{1g} and E_g around 144, 396, 516, and 639 cm^{-1}, respectively. The principal Raman peak shifts to high wave number from TiO_2(SC), $TiO_{2-y}F_y$(SC), $TiO_{2-x}N_x$(SC), to $TiO_{2-x-y}N_xF_y$(SC)-3, indicating the increase of oxygen vacancies [53,54] due to the replacement of O by N- and/or F-dopants in the TiO_2 lattice. Fig. 3(b) also demonstrates that the principal Raman peak shifts positively with the enhanced N-content and F-content in the $TiO_{2-x-y}N_xF_y$(SC) samples, indicating the increase of oxygen vacancies. As shown in Fig. 4, the PL spectra of the undoped and doped TiO_2 samples obtained with excitation wavelength of 280 nm display an emission peak from band edge free excitation around 381 nm [55]. The peak intensity is strongly dependent on the oxygen vacancies since they could capture photoelectrons and thus inhibit the recombination between photo-induced electrons and holes [56,57]. The gradually enhanced peak intensity from TiO_2(SC), $TiO_{2-y}F_y$(SC), $TiO_{2-x}N_x$(SC), to $TiO_{2-x-y}N_xF_y$(SC)-3 further confirms the increase of oxygen vacancies due to the N- and/or F-doping.

The XRD patterns (Fig. 5) demonstrate that the doped and undoped TiO_2 samples calcined at 773 K are present in pure anatase phase, which is consistent with the Raman spectra. Both the N-doping and the F-doping enhance the crystallization degree of anatase, which could account for the higher crystallization degree of $TiO_{2-x-y}N_xF_y$(SC)-3 than either the $TiO_{2-x}N_x$(SC) or the $TiO_{2-y}F_y$(SC). According to Scherrer equation, $d = K\lambda/\beta\cos\theta$, where d is the average crystallite size, K is a constant related to the crystallite shape (0.89) and β is the pure breath of the powder reflection free of the broadening due to instrumental contribu-

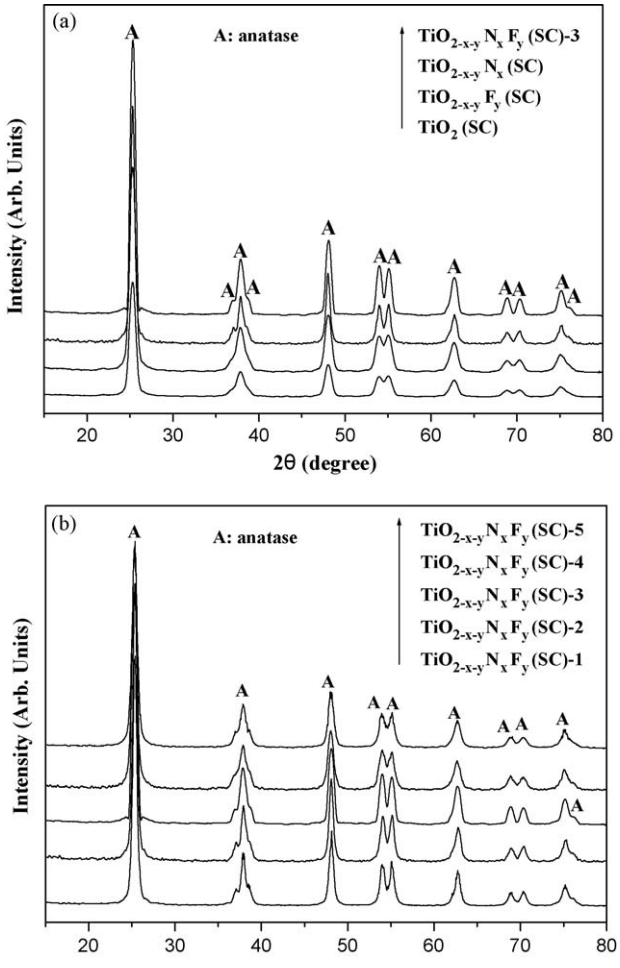

Fig. 5. XRD patterns of different samples calcined at 773 K.

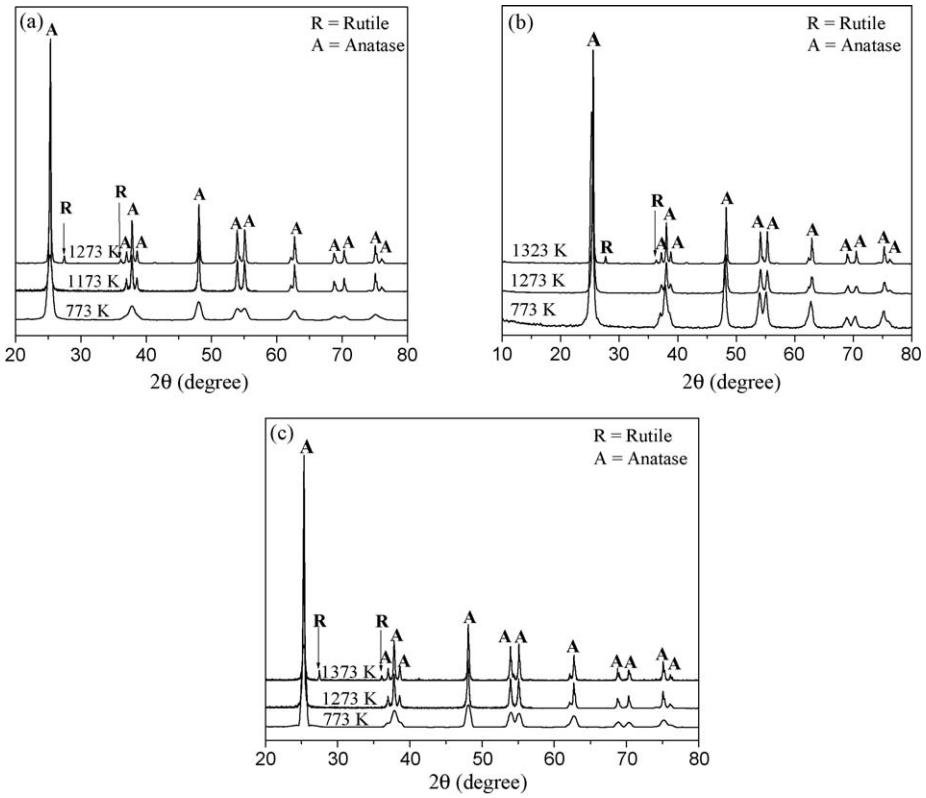

Fig. 6. XRD patterns of (a) $TiO_{2-y}F_y$(SC), (b) $TiO_{2-x}N_x$(SC), and (c) $TiO_{2-x-y}N_xF_y$(SC)-3 samples calcined at elevated temperature.

tions, the crystallite sizes of the TiO_2(SC), $TiO_{2-y}F_y$(SC), $TiO_{2-x}N_x$(SC), and $TiO_{2-x-y}N_xF_y$(SC)-3 samples are determined as 10.7, 11.4, 12.3, and 12.7 nm, showing that the N-doping and F-doping could promote the crystal growth owing to the incorporation of the dopants into the TiO_2 lattice. Fig. 5(b) further illustrates that the crystallite size increases in the order of 11.8, 12.5, 12.7, 13.0, and 13.3 nm with the enhanced content of either the N- or the F-dopants. As shown in Fig. 6, the $TiO_{2-y}F_y$(SC), $TiO_{2-x}N_x$(SC), and $TiO_{2-x-y}N_xF_y$(SC)-3 samples display phase transformation from anatase to rutile at calcination temperature of 1273, 1323, and 1373 K, respectively. Taking into account that the undoped TiO_2(SC) shows phase transformation at 973 K [32], it is obvious that both the N- and the F-doping greatly enhance the thermal stability of anatase owing to the strong crystal distortion force resulting from the incorporation of N- or F-dopants into the TiO_2 lattice via O–Ti–N or O–Ti–F bonding, which could protect the anatase from phase transformation [43]. In addition, the phase transformation temperature of the TiO_2(SC) is nearly 300 K higher than the corresponding TiO_2(DC) obtained via direct calcinations [32], showing the promoting effect of the supercritical treatment on the thermal stability owing to the presence of porous structure which might inhibit the migration and the arrangement of Ti and O atoms to form rutile during calcination [58].

The TEM images (Fig. 7) demonstrate that the TiO_2(DC) is present in the form of nearly shapeless particles with poor crystallization degree. However, the doped and undoped TiO_2 samples obtained under supercritical conditions exhibit regular cubic particles with high anatase crystallization degree, as confirmed by well resolved crystal lattice of 0.35 nm [59] in the attached HRTEM and the well defined diffractional circles in SAED image. This could be attributed to the high pressure and the absence of surface tension under supercritical conditions which could promote the crystal growth and also effectively inhibit the particle agglomeration.

Other structural parameters are summarized in Table 1. The $TiO_{2-x-y}N_xF_y$(SC)-3 exhibits much higher S_{BET} and V_P values than its corresponding one obtained via direct calcinations. This could be attributed to the absence of surface tension under supercritical conditions, so the porous structure in the precursors could be preserved during heating treatments [27,28]. Both the $TiO_{2-x-y}N_xF_y$(SC)-3 and the $TiO_{2-x-y}N_x$(SC) exhibit higher S_{BET} and V_P values than the undoped TiO_2(SC). However, the $TiO_{2-y}F_y$(SC) display almost the same S_{BET} and V_P values as the undoped TiO_2(SC). Thus, one could conclude that the enhanced S_{BET} and V_P are mainly ascribed to the N-doping rather than to the F-doping. A possible reason is that each N could form three O–Ti–N bonds in pyramid and/or dipyramid configurations [32,33], which might generate new porous structure. However, each F could form only one O–Ti–F bond in linear form, which is difficult to induce new porous structure. [13].

The NH_3-TPD profiles (Fig. 8) demonstrate that no significant NH_3 desorption signals are observed in either the undoped TiO_2(SC) or the $TiO_{2-x}N_x$(SC). However, both the $TiO_{2-y}F_y$(SC) and the $TiO_{2-x-y}N_xF_y$(SC)-3 samples display strong NH_3 desorption peaks in the temperature ranging from 400 K to 750 K, obviously owing to the F-doping. The broad temperature range could be attributed to the different kinds of adsorption modes for NH_3, including the chemisorbed NH_3 molecules, the NH_3 molecules combined with the surface-adsorbed F-species via H-bonding [24], and the NH_3 molecules chemically bonded with the F-species incorporated in the TiO_2 lattice [25,60].

The UV–vis DRS spectra (Fig. 9) reveal that the TiO_2(SC) displays no significant absorbance in visible area which could be easily understood by considering its large band gap (3.2 eV). Doping TiO_2 with either the N or the F induces remarkable absorbance for visible lights owing to the appearance of intermediate energy levels via forming O–Ti–F and O–Ti–N bonds, leading to the narrower energy band gap [13,61]. The $TiO_{2-x}N_x$(SC) exhibits

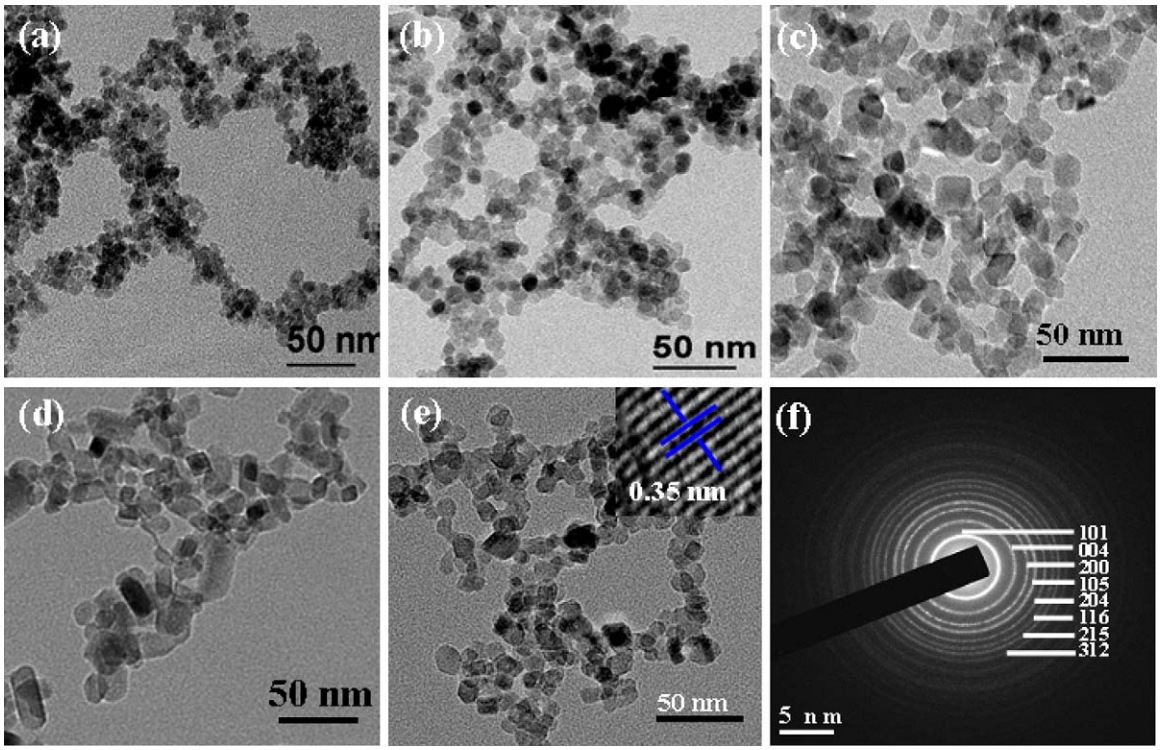

Fig. 7. TEM morphologies of (a) TiO_2(DC), (b) TiO_2(SC), (c) $TiO_{2-y}F_y$(SC), (d) $TiO_{2-x}N_x$(SC), (e) $TiO_{2-x-y}N_xF_y$(SC)-3 samples calcined at 773 K and (f) is the SAED image of the $TiO_{2-x-y}N_xF_y$(SC)-3 and the inset is the HRTEM morphology.

stronger absorbance in visible area than the $TiO_{2-y}F_y$(SC) since each N could form three O–Ti–N bonds [32,33] while each F could form only one O–Ti–F bond [13]. The $TiO_{2-x-y}N_xF_y$(SC)-3 shows the highest visible light absorbance owing to the co-doping effect.

The activities of the as-prepared catalysts are evaluated by using photocatalytic degradation of MB under visible lights ($\lambda > 420$ nm). Fig. 10 shows the dependence of the activity of $TiO_{2-x-y}N_xF_y$(SC)-3 on the calcination temperature. The activity first increases and then decreases with the elevated temperatures. The optimum calcination temperature is determined as 773 K. Since the S_{BET} decreases monotonously with the enhanced calcination temperature, the increase in the activity from 573 K to 773 K could be mainly attributed to the enhanced crystallization degree of anatase phase. The well crystallized anatase might facilitate the transfer of photoelectrons from bulk to surface and thus inhibit their recombination with the photo-generated holes, leading to the enhanced quantum efficiency [62]. Further increase in the calcination temperature causes a slight decrease in the activity due to the rapid decrease of S_{BET}. An abrupt decrease in activity is observed at 1373 K due to the transformation from anatase to rutile.

The catalytic performances of various catalysts calcined at 773 K are summarized in Table 1. The TiO_2(DC), TiO_2(SC) and P25 TiO_2 samples are essentially inactive since they could not be activated by visible lights due to the big energy gap (3.2 eV) [32–35]. The N- and F-doped TiO_2 catalysts display high activity owing

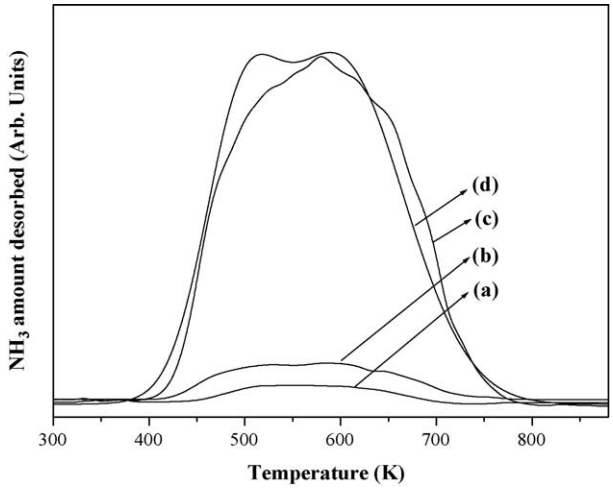

Fig. 8. NH_3-TPD profiles of (a) TiO_2(SC), (b) $TiO_{2-x}N_x$(SC), (c) $TiO_{2-y}F_y$(SC), and (d) $TiO_{2-x-y}N_xF_y$(SC)-3 samples calcined at 773 K.

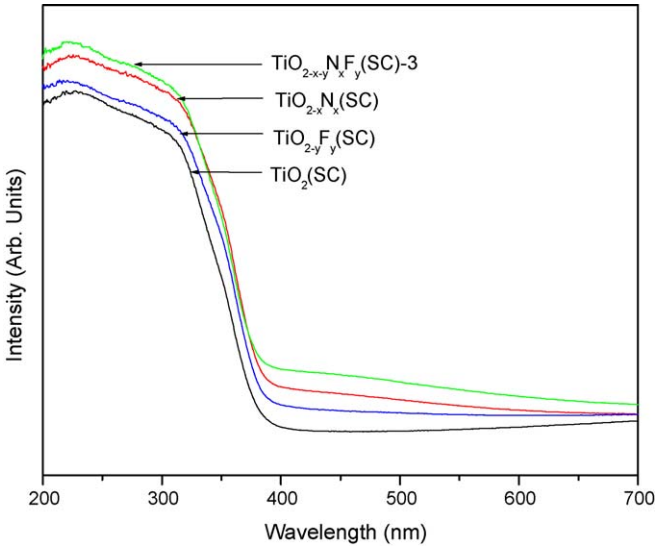

Fig. 9. UV–vis DRS spectra of different samples calcined at 773 K.

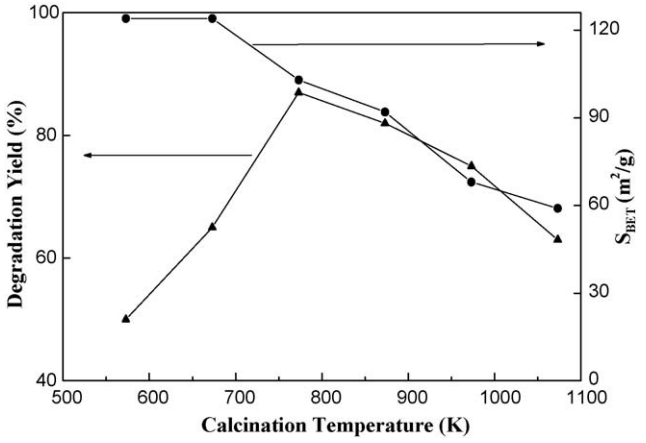

Fig. 10. Dependence of the activity and surface area of the $TiO_{2-x-y}N_xF_y$(SC)-3 on the calcination temperature. Reaction conditions: 0.050 g catalyst, 50.0 mL 0.010 g/L MB, a 500 W Xenon lamp (light intensity = 600 mW/cm^2, wavelength > 420 nm), reaction temperature = 303 K, stirring rate > 800 rpm, reaction time = 3 h.

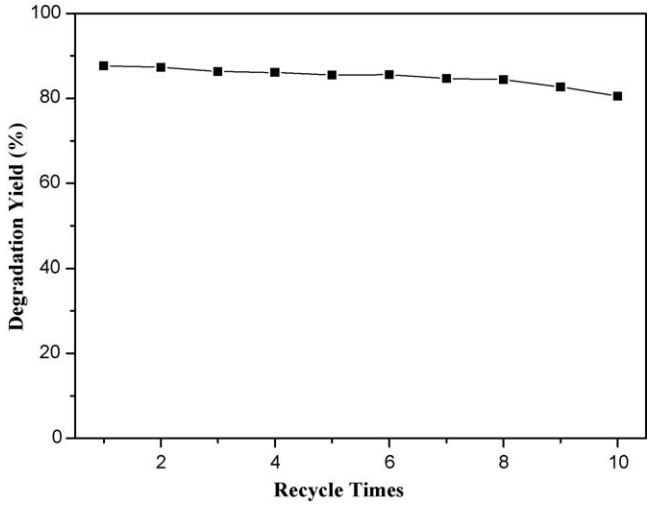

Fig. 11. Recycling test of the $TiO_{2-x-y}N_xF_y$(SC)-3 calcined at 773 K. Reaction conditions are given in Fig. 10.

to the spectral response in visible light area. This could be attributed to the appearance of intermediate energy levels via forming N–Ti–O and F–Ti–O bonds, leading to the narrow energy gaps. The $TiO_{2-x}N_x$(SC) exhibits higher activity than the $TiO_{2-y}F_y$(SC) owing to the higher surface area and more importantly, the stronger absorbance for visible lights (see Fig. 9). The $TiO_{2-x-y}N_xF_y$(SC)-3 exhibits higher activity than either the $TiO_{2-x}N_x$(SC) or the $TiO_{2-y}F_y$(SC) or the mixture of $TiO_{2-x}N_x$(SC)-1 and $TiO_{2-y}F_y$(SC)-1 with the same contents of N- and F-dopants, showing the synergetic promoting effects including the absorbance for visible lights, increased surface acidic sites and oxygen vacancies, enhanced crystallization degree of anatase and high surface area. The activity of $TiO_{2-x-y}N_xF_y$(SC) first increases and then decreases with the enhanced N- and F-contents. The maximum activity is obtained on $TiO_{2-x-y}N_xF_y$(SC)-3. Besides the increase of S_{BET} which is favorable for the adsorption of reactant molecules, the enhanced activity could be attributed to the formation of more intermediate energy levels via forming O–Ti–N and O–Ti–F bonds, leading to the stronger absorbance for visible lights [13,61]. In addition, more oxygen vacancies are induced which could capture photo-induced electrons and thus inhibit their recombination with photo-induced holes, leading to the enhanced quantum efficiency [63]. Furthermore, the higher content of F-dopants could increase surface acidic sites, which could promote the adsorption for MB molecules (see Fig. S1), leading to the enhanced activity [25,64]. At very high N- and F-contents, a large amount of surface-adsorbed N and F-species cover the TiO_2 surface, which might hamper the adsorption for reactant molecules and also capture photo-induced holes acted as the original oxidizing agent in photocatalysis, leading to the low quantum efficiency.

Table 1 also reveals that $TiO_{2-x-y}N_xF_y$(SC) samples exhibit much higher activity than the $TiO_{2-x-y}N_xF_y$(DC) obtained via direct calcination, indicating the promoting effect of supercritical treatment. Besides the higher surface area and the enhanced crystallization degree of anatase, the pressure and temperature under supercritical conditions ensure most of F- and N-dopants incorporated into the TiO_2 lattice. As discussed above, large amount of surface-adsorbed N- and F-species are harmful for photocatalytic reactions.

Besides the higher activity, the $TiO_{2-x-y}N_xF_y$(SC)-3 also shows strong durability during liquid phase photocatalytic degradation of MB. As shown in Fig. 11, the catalyst can be used repetitively for more than 10 times. A slight decrease in activity could be mainly attributed to the loss of catalyst during recycling and washing process. The excellent durability can be attributed to the high thermal and hydrothermal stability, which inhibit the phase transformation from anatase to rutile, the collapse of porous structure, and the leach of N- and F-dopants during liquid phase photocatalytic reactions.

4. Conclusions

This work develops a facile approach to prepare $TiO_{2-x-y}N_xF_y$(SC) by treating the TiO_2 precursor in a NH_4F/ethanol fluid under supercritical conditions. This catalyst exhibits high activity under visible light irradiation owing to the synergetic promotion from supercritical treatment and N- and F-dopants incorporated in the TiO_2 lattice, including the larger surface area, the higher crystallization degree of anatase, the narrower energy band gaps, and the enhanced acidic sites. Other co-doped or multi-doped TiO_2 could also be synthesized based on the present method, which offers more opportunities for designing more powerful photocatalysts.

Acknowledgment

This work was supported by the National Natural Science Foundation of China (20825724), Shanghai Government (S30406, 07dz22303, 0852nm01000, 09YZ162), and Shanghai Normal University (DZL807, SK200838).

Appendix A. Supplementary data

Supplementary data associated with this article can be found, in the online version, at doi:10.1016/j.apcatb.2009.01.019.

References

[1] F. Cesano, S. Bertarione, A. Damin, G. Agostini, S. Usseglio, J.G. Vitillo, C. Lamberti, G. Spoto, D. Scarano, A. Zecchina, Adv. Mater. 20 (2008) 3342.
[2] M. Sathish, B. Viswanathan, R.P. Viswanath, C.S. Gopinath, Chem. Mater. 17 (2005) 6349.
[3] M. Kitano, M. Matsuoka, M. Ueshima, M. Anpo, Appl. Catal. A 325 (2007) 1.
[4] N. Lu, X. Quan, J.Y. Li, S. Chen, H.T. Yu, G.H. Chen, J. Phys. Chem. C 111 (2007) 11836.
[5] R. Asahi, T. Morikawa, T. Ohwaki, K. Aoki, Y. Taga, Science 293 (2001) 269.
[6] H. Choi, M.G. Antoniou, M. Pelaez, A.A. de la Cruz, J.A. Shoemaker, D.D. Dionysiou, Environ. Sci. Technol. 41 (2007) 7530.
[7] C. Chen, H. Bai, C. Chang, J. Phys. Chem. C 111 (2007) 15228.

[8] M. Kitano, K. Funatsu, M. Matsuoka, M. Ueshima, M. Anpo, J. Phys. Chem. B 110 (2006) 25266.
[9] F.H. Tian, C.B. Liu, J. Phys. Chem. B 110 (2006) 17866.
[10] J. Wang, Q. Zhang, S. Yin, T. Sato, F. Saito, J. Phys. Chem. Solids 68 (2007) 189.
[11] W. Ho, J.C. Yu, S. Lee, J Solid State Chem. 179 (2006) 1171.
[12] J.S. Park, W. Choi, Langmuir 20 (2004) 11523.
[13] J.C. Yu, J.G. Yu, W.K. Ho, Z.T. Jiang, L.Z. Zhang, Chem. Mater. 14 (2002).
[14] J.H. Park, S. Kim, A.J. Bard, Nano Lett. 6 (2006) 24.
[15] W.J. Ren, Z.H. Ai, F.L. Jia, L.Z. Zhang, X.X. Fan, Z.G. Zou, Appl. Catal. B 69 (2007) 138.
[16] G. Wu, T. Nishikawa, B. Ohtani, A. Chen, Chem. Mater. 19 (2007) 4530.
[17] A. Ghicov, J.M. Macak, H. Tsuchiya, J. Kunze, V. Haeublein, L. Frey, P. Schmuki, Nano Lett. 6 (2006) 1080.
[18] M. Mrowetz, W. Balcerski, A.J. Colussi, M.R. Hoffmann, J. Phys. Chem. B 108 (2004) 17269.
[19] K.S. Yang, Y. Dai, B.B. Huang, J. Phys. Chem. C 111 (2007) 12086.
[20] A. Hattori, K. Shimota, H. Tada, S. Ito, Langmuir 15 (1999) 5422.
[21] R. Bacsa, J. Kiwi, T. Ohno, P. Albers, V. Nadtochenko, J. Phys. Chem. B 109 (2005) 5994.
[22] X.F. Chen, X.C. Wang, Y.D. Hou, J.H. Huang, L. Wu, X.Z. Fu, J. Catal 255 (2008) 59.
[23] Y. Guo, X.W. Zhang, G.R. Han, Mater. Sci. Eng. B 135 (2006) 83.
[24] D. Li, H. Haneda, S. Hishita, N. Ohashi, Chem. Mater. 17 (2005) 2588.
[25] D. Li, H. Haneda, S. Hishita, N. Ohashi, N.K. Labhsetwar, J. Fluorine Chem. 126 (2005) 69.
[26] A. Borras, C. Lopez, V. Rico, F. Gracia, A.R. Gonzalez-Elipe, E. Richter, G. Battiston, R. Gerbasi, N. McSporran, G. Sauthier, E. Gyo1rgy, A. Figueras, J. Phys. Chem. C 111 (2007) 1801.
[27] K. Watanabe, D. Menzel, N. Nilius, H.J. Freund, Chem. Rev. 106 (2006) 4301.
[28] T.L. Thompson, J.T. Yates, Chem. Rev. 106 (2006) 4428.
[29] V. Gourinchas-Courtecuisse, F. Bocquet, K. Chhor, C. Pommier, J. Supercrit. Fluids 9 (1996) 222.
[30] G.M. An, W.H. Ma, Z.Y. Sun, Z.M. Liu, B.X. Han, S.D. Miao, Z.J. Miao, K.L. Ding, Carbon 45 (2007) 1795.
[31] C. Aymonier, A. Loppinet-Serani, H. Reveron, Y. Garrabos, F. Cansell, J. Supercrit. Fluids 38 (2006) 242.
[32] H.X. Li, J.X. Li, Y.N. Huo, J. Phys. Chem. B 110 (2006) 1559.
[33] Y.N. Huo, Z.F. Bian, X.Y. Zhang, Y. Jin, H.X. Li, J. Phys. Chem. C 112 (2008) 6546.
[34] H.X. Li, X.Y. Zhang, Y.N. Huo, J. Zhu, Environ. Sci. Technol. 41 (2007) 4410.
[35] Y.N. Huo, X.Y. Zhang, Y. Jin, J. Zhu, H.X. Li, Appl. Catal. B 83 (2008) 78.
[36] Operator's reference manual for PHI PC windows software Version 1.2b, Physical Electronic Division, Perkin–Elmer, p. 254.
[37] Y. Kuroda, T. Mori, K. Yagi, N. Makihata, Y. Kawahara, M. Nagao, S. Kittaka, Langmuir 21 (2005) 8026.
[38] C.P. Sibu, S.R. Kumar, P. Mukundan, K.G.K. Warrier, Chem. Mater. 14 (2002) 2876.
[39] Y. Tanaka, M. Suganuma, J. Sol–Gel Sci. Technol. 22 (2001) 83.
[40] B. Gao, Y. Ma, Y. Cao, W. Yang, J. Yao, J. Phys. Chem. B 110 (2006) 14391.
[41] S. Sakthivel, M. Janczarek, H. Kisch, J. Phys. Chem. B 108 (2004) 19384.
[42] J.A. Navio, C.C. Cerrillos, C. Real, Surf. Interface Anal. 24 (1996) 355.
[43] L.N. Ignateva, S.A. Polishchuk, T.F. Antokhina, V.M. Buznik, Glass Phys. Chem. 30 (2004) 139.
[44] K. Nakamoto, Infrared Spectra of Inorganic and Coordination Compounds, Wiley, New York, 1970.
[45] X.F. Song, L. Gao, Langmuir 23 (2007) 11850.
[46] O. Diwald, T.L. Thompson, E.G. Goralski, S.D. Walck, J.T. Yates, J. Phys. Chem. B 108 (2004) 52.
[47] X.B. Chen, C. Burda, J. Phys. Chem. B 108 (2004) 15446.
[48] Y. Cong, J.L. Zhang, F. Chen, M. Anpo, D.N. He, J. Phys. Chem. C 111 (2007) 10618.
[49] C. Valentin, G. Pacchioni, A. Selloni, J. Phys. Chem. B 109 (2005) 11414.
[50] N.C. Saha, H.G. Tompkins, J. Appl. Phys. 72 (1992) 3072.
[51] H. Park, W. Choi, J. Phys. Chem. B 108 (2004) 4086.
[52] Y.Q. Wang, P.M.A. Sherwood, Chem. Mater. 16 (2004) 5427.
[53] K.R. Zhu, M.S. Zhang, Q. Chen, Z. Yin, Phys. Lett. A 340 (2005) 220.
[54] H.M. Liu, W.S. Yang, Y. Ma, Y.A. Cao, J.N. Yao, J. Zhang, T.D. Hu, Langmuir 19 (2003) 3001.
[55] J.G. Yu, J.C. Yu, M.K.P. Leung, W.K. Ho, B. Cheng, X.J. Zhao, J.C. Zhao, J. Catal. 217 (2003) 69.
[56] H. Tang, K. Prasad, R. Sanjines, P.E. Schmidd, F.J. Levy, Appl. Phys. 75 (1994) 2042.
[57] H. Tang, H. Berger, P.E. Schmidd, F. Levy, G. Burri, Solid State Commun. 87 (1993) 847.
[58] T. Osaki, K. Nagashima, K. Watari, K. Tajiri, J. Non-Crystal. Solids 353 (2007) 2436.
[59] Z.Y. Liu, X.T. Zhang, S. Nishimoto, M. Jin, D.A. Tryk, T. Murakami, A. Fujishima, Langmuir 23 (2007) 10916.
[60] G. Busca, H. Saussey, O. Saur, J.C. Lavalley, V. Lorenzelli, Appl. Catal. 14 (1985) 245.
[61] H. Irie, Y. Watanabe, K. Hashimoto, J. Phys. Chem. 107 (2003) 5483.
[62] H.C. Choi, Y.M. Jung, S.B. Kim, Vib. Spectrosc. 37 (2005) 33.
[63] T. Toyoda, T. Hayakawa, K. Abe, T. Shigenari, Q. Shen, J. Lumin. 87 (2000) 1237.
[64] S.R. Morrison, Surf. Sci. 50 (1975) 329.